PERGAMON

International Journal of Heat and Mass Transfer 45 (2002) 4831–4845

International Journal of HEAT and MASS TRANSFER

www.elsevier.com/locate/ijhmt

Numerical simulation of steady state heat transfer in a ceramic-coated gas turbine blade

N. Asok Kumar [a], S.R. Kale [b,*]

[a] Department of Mechanical Engineering, College of Engineering, Thiruvananthapuram 695016, India
[b] Department of Mechanical Engineering, Indian Institute of Technology Delhi, New Delhi 110016, India

Received 24 June 1999; received in revised form 16 April 2002

Abstract

As gas turbine entry temperature (TET) increases, thermal loading on first stage blades increases and, therefore, a variety of cooling techniques and thermal barrier coatings (TBCs) are used. In the present work, steady state blade heat transfer mechanisms were studied via numerical simulations. Convection and radiation to the blade external surface were modeled for a super alloy blade with and without a TBC. The effects of surface emissivity changes, partial TBC coatings and uncertainties in external heat transfer coefficient were also simulated. The results show that at 1500 K TET, radiation heat transfer rate from gas to an uncoated blade is 8.4% of total heat transfer rate which decreases to 3.4% in the presence of a TBC. The TBC blocks radiation, suppresses metal temperatures and reduces heat loss to the coolant. These effects are more pronounced at higher TETs. With selective coating, substantial local temperature suppression occurs. In the presence of radiation and/or TBC, the uncertainties in convection heat transfer coefficient do not have a significant effect on metal temperatures.

Keywords: Gas turbine blade; Thermal barrier coating; Heat transfer; Simulation; Radiation; Uncertainties

1. Introduction and literature review

The continuing thrust towards higher thermal efficiencies of gas turbines has manifested in a continuous increase in the turbine entry temperature (TET). As a result of this trend industrial gas turbines, such as, those used in combined cycle power plants, with TETs of 1400 °C are being manufactured and efforts to attain TET of 1500 °C are under way [1] and, more recently, TETs of 1700 °C have been conceptualized [2].

The hot gas path components, in particular first stage nozzle and rotor blades, have to withstand these elevated temperatures which necessitates effective cooling techniques. Traditional cooling methods of transpiration cooling, showerhead cooling and internal cooling, amongst others, are effective in maintaining allowable blade temperatures but at the expense of cycle efficiency due to dilution of hot gas with coolant, aerodynamic mixing loss and rotor blade pumping loss, amongst others. Reduction, if not elimination, of these losses is essential to achieve cycle efficiencies of 60% [2] which is possible by providing thermal barrier coating (TBC).

The important research areas related to heat transfer to a gas turbine blade include, external and internal heat transfer coefficient predictions, metal temperature distribution, blade cooling methods, rotation effects, and ceramic coatings, amongst others. External convection depends upon the development of the boundary layer on the blade surface, which is a complex phenomenon, and there is considerable uncertainty associated with both numerical predictions and experimental measurements. Most studies have thus far been limited to convection analysis assuming that radiation heat transfer is relatively unimportant.

Research on heat transfer through ceramics/ceramic coatings has focussed on the prediction of stresses and crack growths. There are relatively few studies on

* Corresponding author.
E-mail addresses: asoknak@hotmail.com (N. Asok Kumar), srk@mech.iitd.ernet.in (S.R. Kale).

0017-9310/02/$ - see front matter
PII: S0017-9310(02)00190-4

Nomenclature

h	convection heat transfer coefficient
k	thermal conductivity
l	direction cosines
$[K]$	conduction matrix
$[N]$	matrix of shape (nodal interpolation) functions
N_i	interpolation function associated with the ith nodal degree of freedom
P	number of nodes
$\vec{P}$	additional heat flux vector
S	distance from leading to trailing edge along pressure/suction surfaces
$\vec{T}$	vector of unknown nodal temperatures
T	temperature
V	volume
X	distance along the pressure/suction surface from the leading edge
x, y	coordinate axes

Greek symbols

ρ	density
σ	Stefan–Boltzmann constant
ε	emissivity
τ	turbulence level

Subscripts

∞	surrounding fluid
c	coolant
g	gas
i	node designation
r	radiation
s	surface

Superscript

e	element

prediction of blade temperatures. Experimental measurements are very difficult to make and, further, generally not reported in literature in detail. The first stage stationary vane and rotating blade for a 1500 °C class, high efficiency, heavy duty gas turbine using full-coverage film cooling (FCFC) on a directionally solidified (DS) nickel base super alloy with zirconia TBC have been experimentally studied for creep and thermal fatigue [1].

The characteristics of several cooling schemes and the performance of TBCs for the first stage nozzles and blades for an advanced power generation engine with TET 1400 °C have also been investigated [3]. The TBC thickness was 0.3 mm or 0.4 mm of partially stabilized zirconium oxide and metal temperature reduction between 40 and 60 °C were obtained for the first stage nozzle and blade, respectively. In a continuing study [4], the effects of 0.2 mm thick ceramic coating on cooling effectiveness were studied. An experimental and numerical estimate (using a one-dimensional model) of the heat flow reduction due to a 0.5 mm partially stabilized zirconia TBC on an air cooled cylindrical specimen showed that at 1093 °C the calculated reduction in heat flow was 64.3% as against a measured reduction of 68.8% [5].

Several researchers have used the finite element technique for blade heat transfer analysis. Three-dimensional steady state metal temperatures in a blade were computed using a generalized finite element code [6]. The FEM used 8-node prism elements and 4-node tetrahedral elements with an adaptive mesh refinement scheme. Radiation heat transfer was not included and their results suggest that spatial resolution was not very high. The FEM analysis has also been used to study steady state and transient temperature variations in a solid turbine blade without any coolant channels and TBC [7] and for a scramjet engine strut [8,9]. The FEM technique has been used for design, analysis and life prediction [10,11]. Studies on the mechanical properties of TBCs have addressed issues relating to low and elevated temperature characteristics [12] and application of coatings [13].

The thermal characteristics of a water-cooled nozzle blade and steam-cooled rotor blade with and without TBC have been studied numerically [2] to study the feasibility of water/steam cooling systems for a 1700 °C TET hydrogen burning combustion steam turbine. Using TBC and very limited film cooling they have predicted that thermal efficiency of up to 60% is attainable if coolant does not mix with the main stream. Losses associated with extensive film cooling, viz., dilution of hot gas with coolant, aerodynamic mixing loss, and rotor blade pumping loss are almost completely eliminated in this manner. Their nozzle blade material was a copper alloy with 0.3 mm TBC and bond layer. A multihole cooling design was envisaged and the temperature distribution using a simple convection–conduction model was used for predicting blade temperatures.

These developments indicate that ceramic-coated blades without extensive film cooling are necessary for achieving higher efficiencies. This research was undertaken to study the effects of various parameters which affect such a blade, viz., radiation, which has not been considered so far, surface properties of coating which

affects radiation heat transfer and above all, uncertainties in the pressure and suction side heat transfer coefficients.

2. Heat transfer model

In this study, a FEM based numerical scheme was developed for a two-dimensional blade [14] and salient features are given below.

2.1. Governing equations and boundary conditions

Within a two-dimensional blade of isotropic material, the steady state heat transfer without heat sinks and sources is given by

$$\frac{\partial}{\partial x}\left(k\frac{\partial T}{\partial x}\right)+\frac{\partial}{\partial y}\left(k\frac{\partial T}{\partial y}\right)=0 \tag{1}$$

For ceramic-coated blades, there is a spatial variation in local thermal properties because of different materials, viz., ceramic TBC and base super alloy. The range of temperatures encountered in blades is large due to which there are significant variations in the properties, thermal conductivity and specific heat, in particular, for both the super alloy and the ceramic. The boundary conditions arise at the blade pressure and suction surfaces, which are exposed to the gas stream, and at the internal coolant passage surfaces which exchange heat with the coolant air. The pressure and suction surfaces are heated by convection from the free stream gases. This heat transfer has been modeled by assuming constant free stream temperature, same as TET, and a local average heat transfer coefficient which varies along the surfaces. A parallel heat transfer mechanism to the external surfaces is by radiation from the gases and other surfaces. This complex radiation phenomena has been simplified for the present work by modeling the radiation environment as an all enclosing large surface whose temperature is same as the TET. The radiation formulation is based on the fact that the blade does not see itself, an assumption that will not result in any significant error due to the small value of this shape factor. Thus, at the external surface, the local boundary condition becomes

$$k\frac{\partial T}{\partial x}l_x+k\frac{\partial T}{\partial y}l_y+h_x(T_\infty-T_s)+h_r(T_\infty-T_s)=0 \tag{2}$$

where radiation heat transfer coefficient is given by

$$h_r=\varepsilon\sigma(T_\infty^2+T_s^2)(T_\infty+T_s) \tag{3}$$

Convection at internal passage surfaces is a complex phenomenon of forced and natural convection and pin fin cooling. The air temperature increases as it flows through the passages making the problem highly three-dimensional. This complex phenomenon has been modeled as a uniform flow in each passage, at the same temperature, with a uniform heat transfer coefficient, h_i. The boundary condition at the internal surface becomes

$$k\frac{\partial T}{\partial x}l_x+k\frac{\partial T}{\partial y}l_y+h_x(T_s-T_c)=0 \tag{4}$$

2.2. Finite element formulation

The finite element formulation was developed using a weighted residual method. Application of the Galerkin method starts by setting the integral of a weighted residue over the domain of the element to zero by taking some interpolation function as the weights, N_i. Mathematically, it is described as follows:

$$\int_{V^e}N_i\left[\frac{\partial}{\partial x}\left(k\frac{\partial T^e}{\partial x}\right)+\frac{\partial}{\partial y}\left(k\frac{\partial T^e}{\partial y}\right)\right]\mathrm{d}V=0,\quad i=1,2,3,\ldots p \tag{5}$$

By using Green's theorem for expanding the terms inside the above integral and rearranging the terms, the element equations are obtained in matrix form:

$$[K]\vec{T}=\vec{P} \tag{6}$$

These element equations were then assembled to form the global equations, which were solved after incorporating the boundary conditions. For radiation boundary conditions, two additional matrices were incorporated along with the $[K]$ and $\vec{P}$ matrices of Eq. (6). Upon assembling the elemental matrices, the resultant global system of equations is a set of non-linear algebraic equations. The non-linearity arises due to the radiation term and also due to the temperature dependant material properties. From Eq. (3), it can be seen that the local radiation heat transfer coefficient depends on the local surface temperature, T_s, an unknown itself. In the FEM scheme, the solution was arrived at by initially setting h_r to zero, calculating T_s and then recalculating h_r; this iterative procedure was repeated until convergence. Another iterative procedure was used for updating thermal properties.

2.3. Code development

Based on the finite element formulation, a versatile computer code was developed to study the two-dimensional heat transfer in the blade. The code allowed input of any combination of blade shape and size, non-linear material properties and boundary conditions. The discretized blade geometry was redrawn several times to eliminate elongated elements. The blade geometry was discretized into a large number, 1158 elements with 691 nodes, of three-noded triangular elements (Fig. 1), for higher accuracy. A refined mesh was used in regions where acute changes in geometry, boundary conditions,

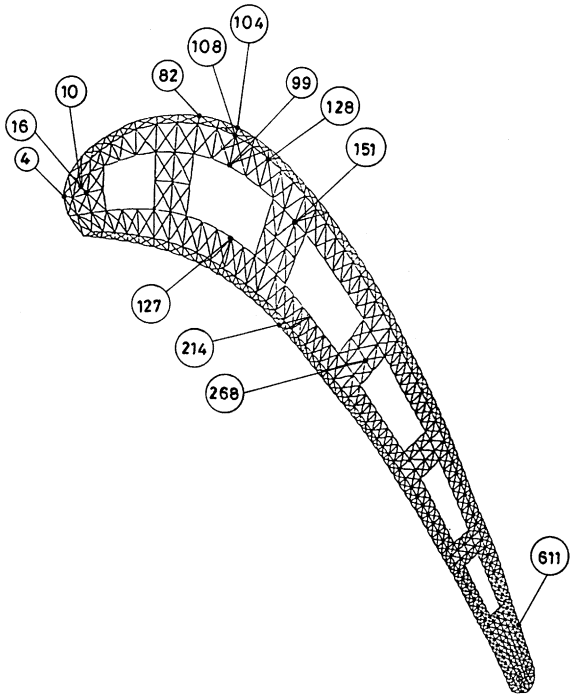

Fig. 1. Discretization of blade cross-section and location of selected nodes.

loading, material properties, or solution occur. In the absence of data representative of actual engine conditions for code validation, the exact solutions for a hollow cylinder were compared with the code output and an excellent match was observed.

2.4. Blade data and simulation parameters

For comparison, sets of conditions were selected and designated as the base case, which was a coated blade with external convection and radiation. The material was super alloy MAR-M200 [15], a widely used blade material, coated with a 0.6 mm thick TBC of Yttria partially stabilized zirconia [16–18]. The emissivity of MAR-M200 was taken as 0.7 and that of zirconia as 0.31. The blade aerodynamic profile [19] shown in Fig. 1 was used in all simulations. For this same profile, five sets of external heat transfer data, four from experiments [19] and one from computation [20] were available; these are shown in Fig. 2. For the base case, experimental data [19] at 4% turbulence and Reynolds number 1.3×10^6 were used. A TET of 1500 K was used for the base case. On the basis of data available in literature, coolant side heat transfer coefficient was calculated as 1200 $W/m^2 K$ and coolant temperature was taken as 850 K. These coolant side parameters vary locally within each passage and, also, from one passage to another due to variations in blade geometry, internal structures, passage sides and areas, amongst others. Their effects on blade temperatures were simulated, particularly, in respect of variations in average coolant heat transfer coefficient and side-to-side variations due to blade rotation. As indicated below, these variations did not have any significant impact on coated blades and, hence, the above values were used in the simulations.

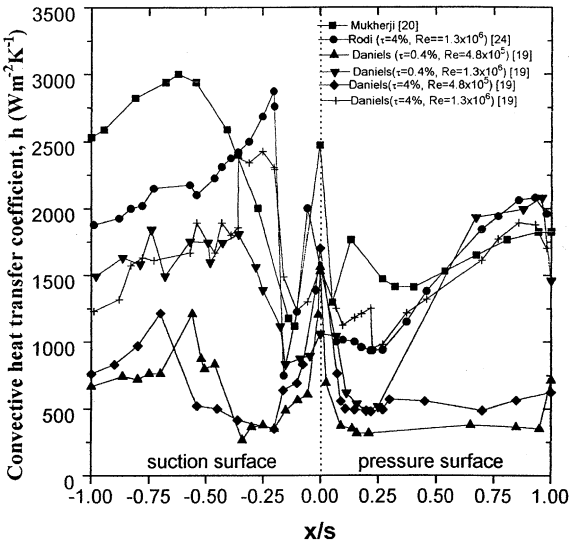

Fig. 2. Convection heat transfer coefficient variation on the blade.

3. Results and discussion

Simulations were performed with the data described above in Section 2.4. For the base case, the effects of coolant heat transfer coefficient were studied by varying the ratio of coolant to average gas side heat transfer coefficients between 0.2 and 1.6. Cooling effectiveness increased by about 10% for uncoated blades but had no impact on coated blades. Rotation induced side-to-side variation in coolant heat transfer coefficient was simulated and it had almost no effect on temperatures inside the coated blade. Hence, results presented are with the data described in the previous section. After simulations of the base case, effects of coatings, radiation, surface emissivity, selective coatings on blade and uncertainty in external convection heat transfer coefficient were computed individually. A TET range from 900 to 1600 K was considered. Some simulations were performed at even higher temperatures for the fully coated blade alone because without coating metal temperatures approach the super alloy melting point. Simulations for the uncoated blade were performed by assigning super alloy

properties to the entire blade, however, external surface and coolant passage geometry were not altered.

3.1. Heat flux vectors and nodal temperatures

Heat flux vectors for the base case are shown in Fig. 3(a). Their magnitudes and directions are consistent with expected heat flow directions in all regions of the blade. The leading and trailing regions of the blade are subjected to very high and very low temperature gradients, respectively, and thus, are prone to errors due to mesh generation (blade discretization) and due to the numerical technique employed. Fig. 3(b) and (c) show the heat flux vectors in the leading and trailing regions, respectively, and these are consistent with expected heat flow directions. The heat flux vectors in the absence of any coating were also consistent with expected heat flow directions in all regions. These heat flux vectors serve as one test on the mesh; additional tests were carried out to optimize the mesh and to minimize numerical errors. The mesh was optimized through a series of iterations for eliminating long aspect ratio elements (angles less then 30° or greater than 120° or both). This process also reduced numerical errors. Subsequently, an overall energy balance was ascertained for various conditions by comparing heat transfer into the blade at the external surfaces with outflow at the coolant passage surfaces. This agreement was within $\pm 11\%$ and it was traced to numerical uncertainties arising at the external surface due to small differences in temperatures between the gas and the local surface accompanied by large values of gas side local heat transfer coefficient, integrated over a large area. This agreement is within reported values of uncertainties from experimental studies.

In the leading edge region, just under the TBC, the effect of TET on the temperature at node 10 (Fig. 1) is shown in Fig. 4(a). The suppression in metal temperature due to the application of the TBC is seen, the magnitude of which increases as TET increases. At 1600 K, the suppression is 58 and 94 K, without and with radiation, respectively. The trend is similar for node 151 (Fig. 1) located in the metal between two coolant passages (see Fig. 4(b)). The magnitude of temperature suppressions at 1600 K TET is 75 and 101 K, without and with radiation, respectively. These data indicate the range of metal temperature suppression attainable by applying TBC. These trends and order of magnitude of temperature suppression are also noticed at node 99 (Fig. 4(c)), in the metal and located on the coolant passage.

The application of a TBC causes the surface temperature to increase. This effect is seen in Fig. 4(d) for node 104 located on the suction surface at x/s of 0.25. The temperature rise is 29 K for the base case and 46 K without radiation, a trend observed over most of the pressure and suction surfaces. The leading and trailing edge regions run hotter because of which the surface temperature elevation due to the TBC is not pronounced,

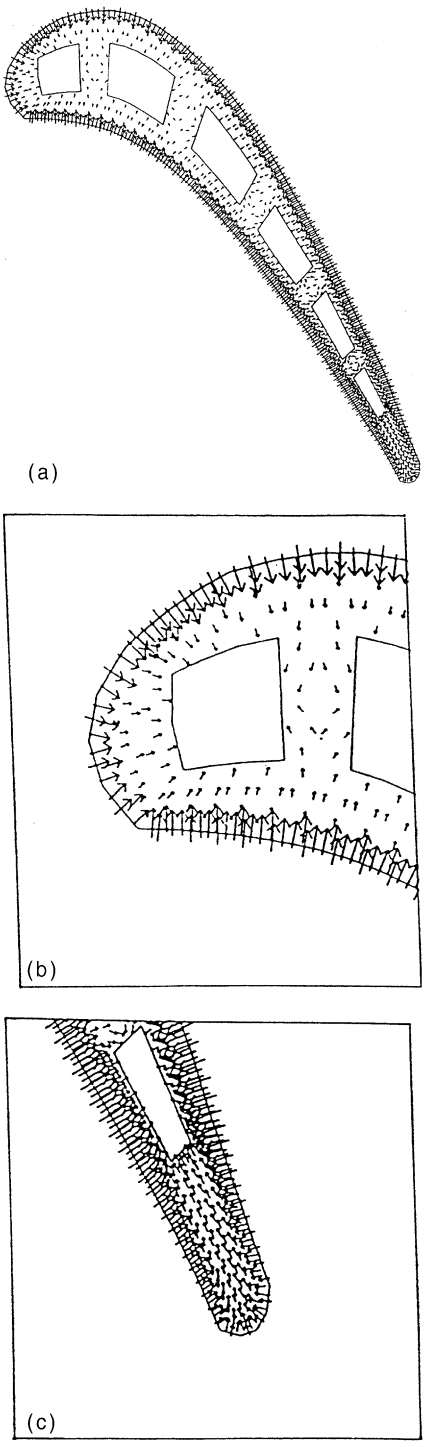

Fig. 3. Heat flux vectors (a) for the coated blade, (b) near the leading edge for the coated blade, (c) near the trailing edge for the coated blade, in the presence of radiation.

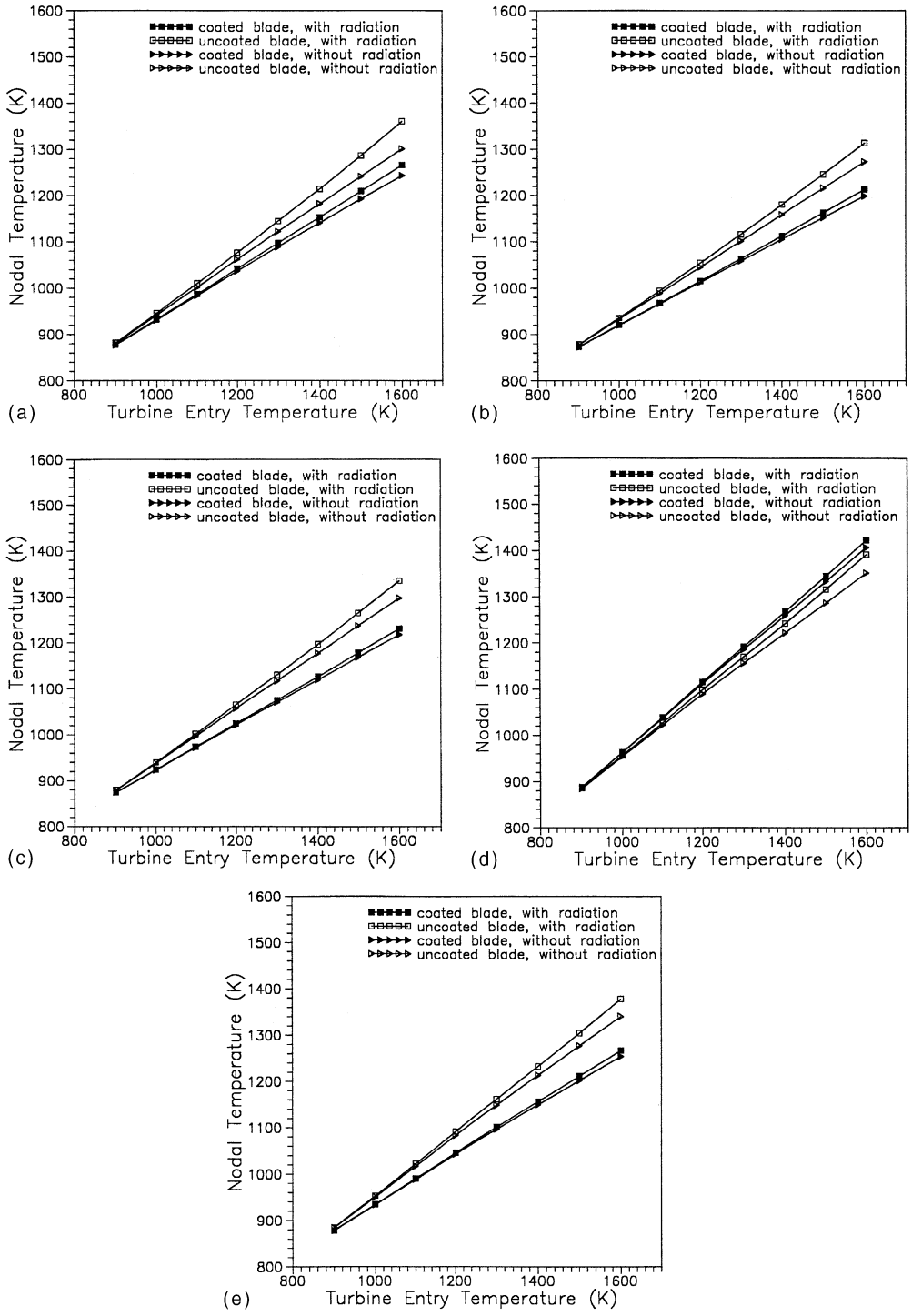

Fig. 4. Effect of TBC and radiation on the temperature at (a) node 10, (b) node 151, (c) node 99, (d) node 104, (e) node 128.

about 9 K for base case. Without radiation, these regions experience temperature rise between 13 and 25 K when TBC is applied.

The build-up of stresses at the TBC–super alloy interface is strongly affected by the local temperature gradients. Node 128 (Fig. 1) is one such node at the

interface on the suction side and its temperature at different TETs is shown in Fig. 4(e). For the base case, the nodal temperature is 1212 and 1202 K in the absence of radiation. In the absence of the coating, the nodal temperature is 1305 and 1277 K without radiation. There is, thus, substantial temperature suppression due to the TBC which is weakly affected by radiation. The temperature gradients normal to the local suction surface are 240 K/mm in the TBC and 19 K/mm in the super alloy. Similar nodes located in the proximity of the coolant passage can be expected to experience largest temperature gradients and, hence, large thermal stresses. In the conceptual design of 1700 °C hydrogen combustion turbine [2], much steeper temperature gradients are envisaged, 2000 K/mm for rotor blade and 4000 K/mm for the nozzle. However, the material contemplated is copper in which such large variations are possible, unlike nickel base super alloys studied here.

A general trend observed in Fig. 4(a–e) is that as TET increases, the nodal temperatures increase in an almost linear manner. The data also shows that the TBC is also very effective in blocking radiation heat transfer, i.e. the additional thermal load does not result in proportional increase in nodal temperatures in the super alloy.

In the only experimental data available for comparison [3], metal temperatures were measured on a MAR-M247 blade coated with 0.4 mm thick ceramic (ZrO_2–Y_2O_3) and a NiCoCrAlY bond layer. At 1300 °C TET and 360 °C coolant temperature, metal temperature at a node on the coolant passage decreased from 754 to 694 °C, a decrease of 60 °C attributed to the TBC. Comparable nodes in the present geometry are nodes 127 and 214, shown in Fig. 1. When same TET and coolant temperature were used, temperatures at node 127 for coated and uncoated blades were 1017 and 1128 K, and at node 214 they were 1041 and 1152 K, a decrease of 111 K at both nodes. These temperature values are slightly different from the experimental data [3] primarily due to the thicker coating used in the simulation. At a lower TET of 800 °C [3], a smaller suppression of 35 K in temperature is predicted, temperature of node 127 being 800 K for coated blade and 835 K for uncoated blade. The corresponding values for node 214 are 814 K for coated blade and 850 K for uncoated blade, a 36 K decrease in nodal temperature due to TBC. The temperature suppression trend reported from experiments [3] is generally in agreement with the present simulations. The model predictions though not for the same experimental geometry are in fair agreement with the experimental measurements [3].

In the same experiment [3], peak surface temperatures for coated and uncoated blades were measured. A definite value for coated blades has not been indicated due to large scatter in the data attributed to uncertainties in surface emissivity values. Uncoated blades attain peak temperatures in the range 760–800 °C. At 1500 K TET, peak surface temperature from the simulation is 1441 K and at 1800 K it is 1730 K which occur at the trailing edge. These are substantially greater than the measured values [3] because the uncoated blades were cooled by FCFC in addition to a variety of internal cooling techniques.

In another experiment [21], when a full coating of ZrO_2–Y_2O_3 over a NiCoCrAlY bond coat was applied, metal temperature reductions ranging from 28 to 139 °C were observed. Details of the blade geometry and heat transfer coefficients are not given and so it is difficult to compare this data with simulation results. However, the range of metal temperature reduction overlaps with the range predicted by the model. Uncoated blade metal temperatures have been predicted [22] using a one-dimensional model. When TET increased from 1093 to 1371 °C, with coolant temperature 620 °C, the surface metal temperature increased by 167 °C which agrees reasonably with present predictions of 193 °C for mean metal temperature.

3.2. Effectiveness and heat transfer to blade

The parameter used in this study for quantifying blade cooling and/or the mean blade temperature is the effectiveness which has been defined as the ratio of the difference in gas temperature and the mean blade temperature to the difference in gas and cooling air temperature. The mean blade temperature is computed by an area-averaged temperature. Average of nodal temperatures yields very high values of mean blade temperature and, consequently, unrealistically low effectiveness due to the large number of nodes in the trailing edge region which runs very hot.

Figs. 5 and 6 show the variations in effectiveness and heat transfer rate over a range of TET from 900 to 1600 K for the base case and also without the TBC. The TBC significantly increases the effectiveness, from 0.36 to 0.46 at 1500 K. With increase in TET, the effectiveness of both coated and uncoated blades decreases, the reduction being more for the uncoated blade. In other words, the ability of the TBC to protect the base alloy increases with further increase in TET. This effectiveness value for coated blades includes temperatures of the nodes in TBC also, which run hotter as compared to the uncoated case. The average metal temperature based effectiveness is thus greater than the value of 0.46 calculated for the entire blade at 1500 K. With this modification, the effectiveness value is 0.5 suggesting that suppression of metal temperature is very substantial. In the uncoated blade at 1500 K, the heat transfer rate from gas to blade is 44.1 kW/m of blade height and for the coated blade 35.4 kW/m. The coating, thus, cuts down heat loss by almost 20%.

On applying TBC over the entire blade surface, both convection and total heat transfer rates to the blade

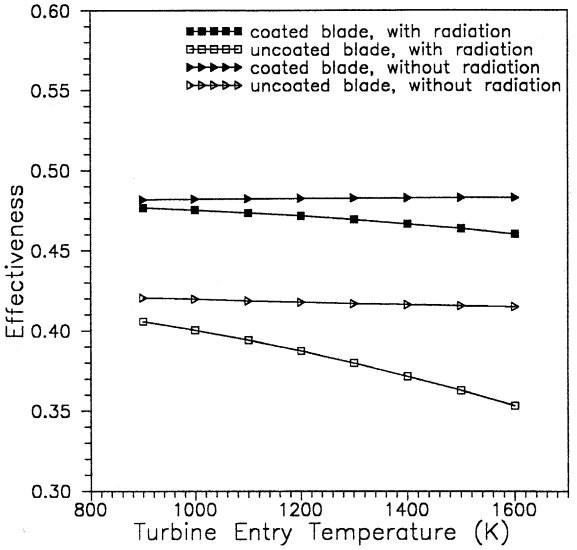

Fig. 5. Effect of TBC and radiation on effectiveness at different TETs.

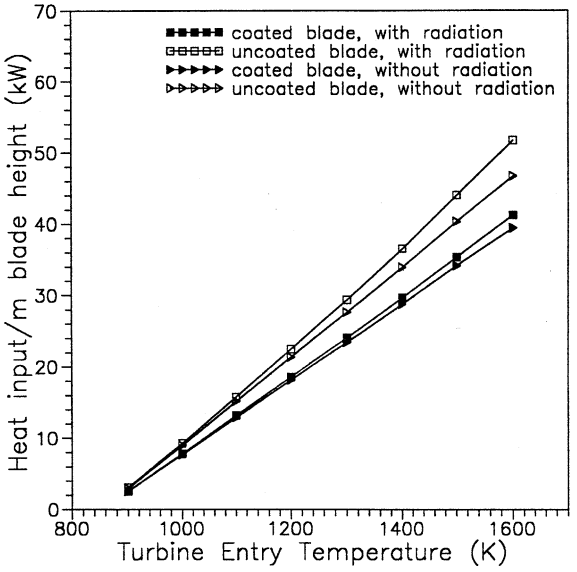

Fig. 6. Effect of TBC and radiation on heat transfer rate at different TETs.

decrease, the latter by 20% at 1500 K TET. The radiation component becomes 1.2 and 2.9 kW/m blade length at TET of 1500 and 1800 K, respectively. These are 3.4% and 5.4% of total heat transfer to the blade, which are significantly smaller than the corresponding values (8.4% and 12.1%) for the uncoated blade. Hence, the TBC not only decreases thermal loading on the blade but also blocks the radiation component very effectively. At elevated TETs, transpiration or film cooling or other convection based cooling techniques are of very limited use in blocking radiation and TBC becomes imperative.

The simulations show an almost 20% decrease in heat loss from hot gases to coolant air due to the presence of full TBC. In such cases, the cooling air flow rate can be reduced for consequent improvement in turbine and cycle thermal efficiency [4]. Experimental measurements of this aspect are rather scarce and, hence, it is difficult to compare the present predictions with data reported in literature. The most definitive study of this effect included development and testing of a hybrid ceramic stator vane for first stage with TET of 1300 °C [23]. The vane was primarily made of ceramic in the form of a shell mounted on a metal core. The metal core was provided with cooling passages through which coolant air at 400 °C was passed. The ceramic temperatures were almost equal to the gas temperature in the TET range of 1000–1300 °C but metal temperatures were about 450 °C which is almost equal to the coolant temperature. Consequently, heat loss was drastically reduced and cooling-to-total air flow ratio of 0.29% was employed which is drastically less than values employed for metal vanes, typically in range of 3%. This experiment clearly brings out the extent of savings possible with thick or nearly complete ceramic vanes. As complete details of their parameters are not available, it is difficult to compare the present simulations with the experimental data. As an extreme case, the simulation was carried out for a full ceramic blade for which heat transfer rate to the blade is 24.7 kW/m which is 30% less than the base case value. For a simpler geometry, hollow INCOLOY 909 cylinder with 500 μm zirconia TBC coating and internally cooled by air, a decrease of 68–75% in heat loss to coolant was measured [5]. A direct comparison of these values with simulations is not possible because the coating thickness and experimental parameters are different from those in the present study. Nevertheless, these studies clearly bring out the tremendous potential of TBC, especially thick coatings.

3.3. Radiation effects

The effectiveness and heat transfer rate to the blade with convection and combined convection–radiation heat transfer from the gas are also shown in Figs. 5 and 6, respectively. For a coated blade at TET of 1500 K, the effectiveness increases from 0.46 to 0.48 when radiation is discounted. The heat transfer rate with radiation is 35.4 kW/m and by neglecting radiation it is 34.2 kW/m, which is 3.4% less. The effect of radiation on coated blades is thus very marginal. At higher temperatures, radiation effect increases as can be seen in Figs. 5 and 6. Fig. 4(a–e) also show that coated blade temperatures are very marginally affected by radiation. When radiation is neglected, for an uncoated blade at 1500 K TET, the effectiveness increases from 0.36 to 0.41 while heat input

decreases from 44.1 to 40.4 kW/m blade length which is 8.4% less. Nodal temperatures increase by 28–45 K when radiation is considered. These effects are accentuated as TET is increased further, as shown in Figs. 4(a–e) and, therefore, radiation contribution is significant for uncoated blades, which is quite unlike a coated blade.

Almost all reported studies on blade heat transfer have concentrated on convection heat transfer from gas to blade. This approach is justifiable at low TETs but at high TETs gas and component surface radiation to the blade could become significant and increase thermal loading on the blade. The simulations show that for uncoated blades, radiation increases thermal loading by 3.7 kW/m of blade height over the convection value at 1500 K TET, a 8.4% increase. At 1800 K, such as being contemplated by designers [1], radiation contribution is 8.2 kW/m which is a 12.1% increase. For these cases, the effectiveness decrease due to radiation is from 0.41 to 0.36 at 1500 K TET and 0.41 to 0.33 at 1800 K TET. The additional loading due to radiation at elevated TETs is, thus, quite significant and needs to be considered while designing blades as also nozzles and other hot gas path components.

Radiation in the turbine is a very complex phenomenon because of the participative nature of the gas and complex shapes and temperatures of the various surfaces seeing each other and the blade. Measurements are particularly difficult because of rotating blades and the harsh environment makes invasive measurements not only difficult, but also error prone. In one study [25] scanning radiation thermometry was used for surface temperature measurements. The measurement required various shape factors for which detailed machine geometry is required; being proprietary nature such data are not available. Also in the absence of detailed experimental conditions, it is not possible to compare the simulations with these experimentally measured temperatures.

3.4. Effect of surface emissivity uncertainty

During operation, the blade surfaces undergo changes due to deposition, corrosion and erosion as a result of which the emissivity of the surface could change. The effect of surface emissivity on effectiveness and heat transfer rate through the blade are shown in Fig. 7(a) and (b), respectively. Data are presented for coated and uncoated blade while considering gas radiation also. A TET of 1500 K has been employed here. When the emissivity of a coated blade increases from 0.2 to 1.0, the effectiveness decreases from 0.47 to 0.43 (Fig. 7(a)), with accompanying heat transfer rate increase from 35 to 38 kW/m (Fig. 7(b)). In case the TBC is not provided, this increase in emissivity decreases effectiveness linearly from 0.4 to 0.34 (Fig. 7(a)), while increasing heat transfer rate from 41.5 to 45.4 kW/m (Fig. 7(b)). Hence,

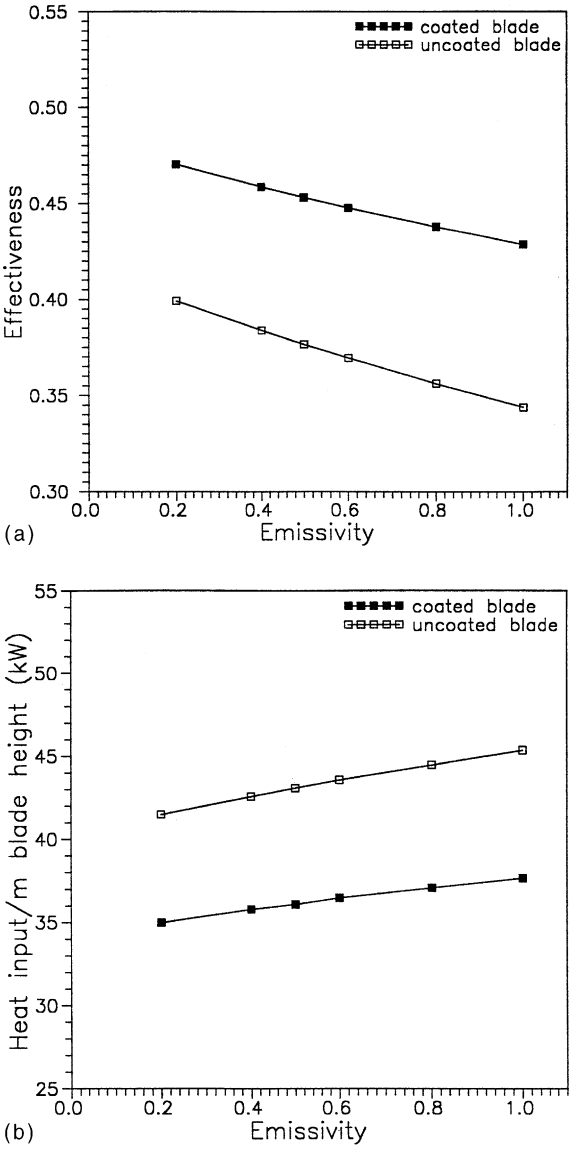

Fig. 7. Effect of emissivity (a) on effectiveness, (b) on heat transfer rate, with and without TBC.

the change in blade heat transfer rate due to changes in emissivity, for either coated or uncoated blades, is less than 10% a value which can be expected to increase at higher TETs. Detailed measurements of emissivity along with documentation of surface physical properties and operating conditions are not available in literature. Hence, a wide range of emissivity values were used for simulations. The corresponding changes in effectiveness as a function of surface emissivity show decreasing effectiveness as the surface approaches a black surface (Fig. 7(a)). Generally, deposits from combustion gases tend to blacken the surface so that its emissivity

increases. As compared to a new blade, a blade after several hours of operation will, therefore, run hotter, i.e., mean metal temperature increases by about 13 K at 1500 K TET for uncoated blades.

3.5. Selectively coated blades

In addition to fully coated blades (base case), selectively coated blades were simulated for studying the local TBC effects. Three cases have been studied, selective coating from the leading edge alone, from the trailing edge alone and from both edges simultaneously. Fig. 8(a) shows the effectiveness changes as TBC is applied separately from leading and trailing edges, respectively. The extent of coating is the x/s value measured from the leading edge (or the trailing edge) on both the pressure and suction surfaces simultaneously. Unity value indicates a fully coated blade, the coating thickness is same (0.6 mm) and external blade geometry is unaltered. The TET is 1500 K, coolant temperature 850 K and radiation has been considered. The corresponding variations in heat transfer rate to the blade are shown in Fig. 8(b). Increasing coating extent has a monotonic influence on increasing the effectiveness, the maximum effectiveness enhancement being for fully coated blades. The variation in effectiveness from 0.36 for uncoated blade to 0.46 for full TBC blade is quite substantial and clearly brings out the benefits of full TBCs. Heat transfer through the blade shows a steady decline as coating extent is increased with fully coated blade resulting in minimal heat transfer.

Ceramic coatings are known to be very brittle and susceptible to cracking and chipping. Thus, larger the ceramic coating greater the chances of failure, even more so when coatings get thicker. One way of minimizing this effect is to selectively apply TBC on those regions of the blade where local temperatures are high. The trailing edge, in particular, is one such region, and another region could be those locations on the pressure and suction surfaces where flow transition occurs. Applying TBC on a section of the surface could not only shield the base metal but also be relatively easy to apply and reduce the cost.

The local effects at six nodes due to selective coating are shown in Fig. 9(a–c). Fig. 9(a) shows that coating to the extent of 7% from the leading edge causes a 24 K rise in the temperature of node 4 located on the nose surface. An additional 27% coating decreases this node temperature by 30 K. Further coatings have no effect on the nodal temperature. In contrast, Fig. 9(a) also shows that node 10, an internal node, experiences a monotonic temperature decrease of about 76 K as coating extent is increased to 34% after which additional coating does not influence it. The benefits of partial coatings are clearly discernable at this node which is located in the metal. Node 104 located on the suction surface, at location x/s

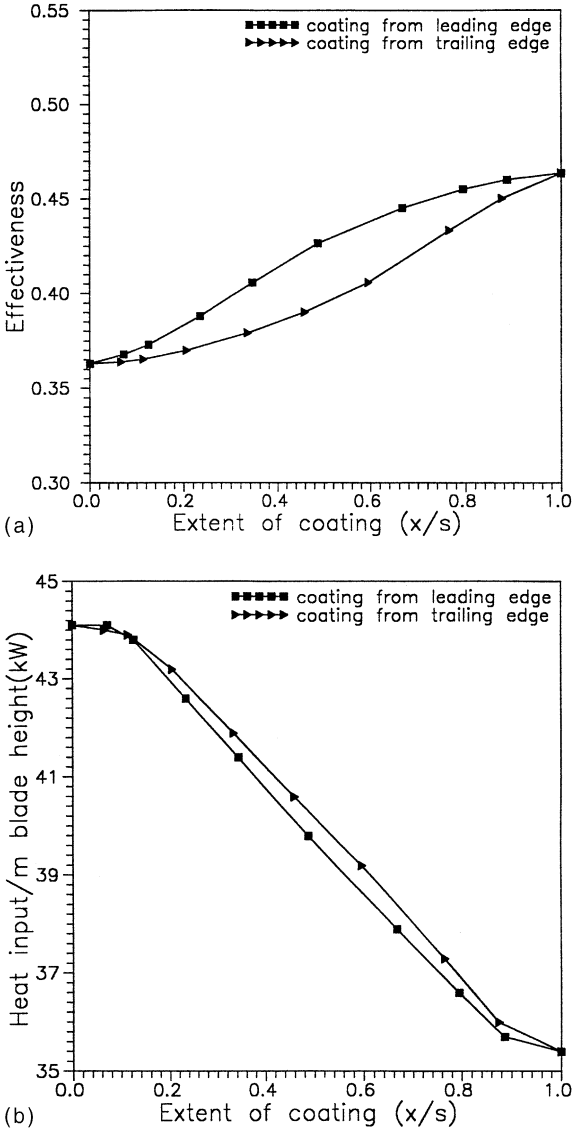

Fig. 8. (a) Effectiveness variation, (b) heat input variation, with selective coating.

of 0.25 from the leading edge, exhibits very interesting behavior as seen in Fig. 9(b). Coating extending up to 12% from the leading edge has almost no influence on this node temperature. Between 12% and 23% coating from the leading edge, the temperature is suppressed by about 18 K. Thereafter, increasing coating to an extent of 48% results in an increase of 53 K over the temperature attained with 23% coating. Additional coating from 48% to 100% has no effect on the nodal temperature. The TBC, thus, has a very marked local influence at this nodal location. Fig. 9(b) also shows the effect on node 108 located on the TBC–alloy interface. The temperature at this node is sensitive to coatings applied

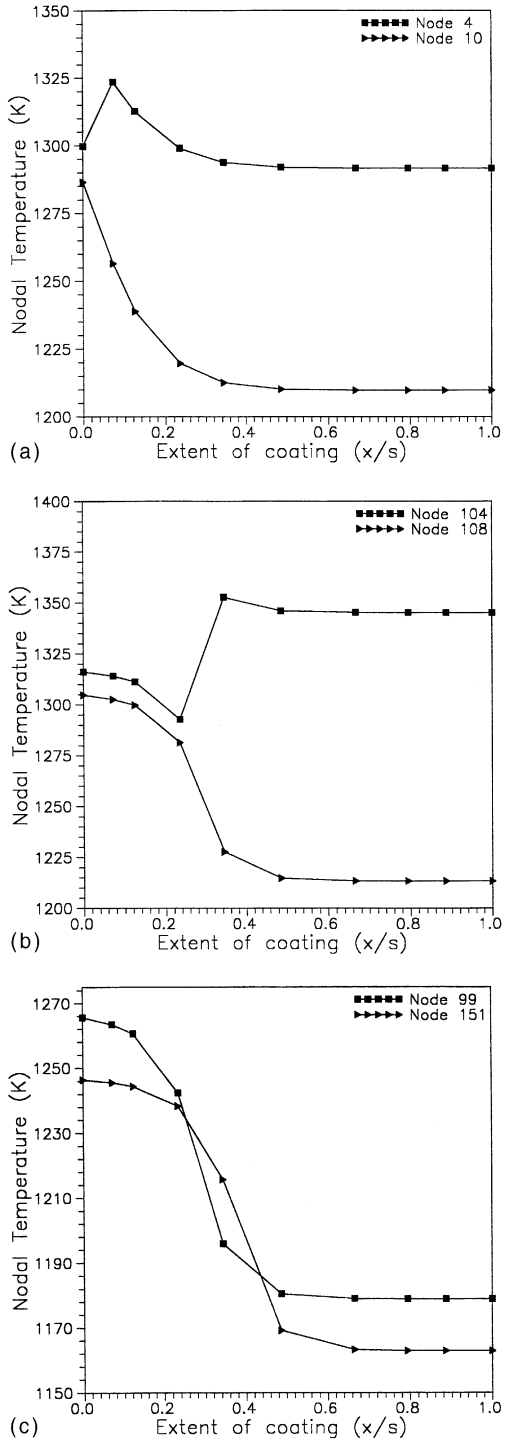

Fig. 9. Effect of selective coating on temperatures at (a) nodes 4 and 10, (b) nodes 104 and 108, (c) nodes 99 and 151.

between 12% and 48% with temperature decrease of almost 85 K. Fig. 9(c) shows the effect of selective coating on node 99 located on the coolant passage and on node 151 located in the super alloy between two coolant passages (Fig. 1). Coatings extending up to 12% from the leading edge suppresses nodal temperatures very weakly but thereafter up to 48% the temperature drops by about 87 K at node 99 and 75 K at node 151. The approximate x/s location of nodes 99 and 151 are 0.26 and 0.37, respectively, which is where the influence is strongest. The trailing edge region is affected very marginally by the TBC, the maximum suppression being only 11 K. A similar effect is observed when the coating is applied from the trailing edge extending towards the leading edge. These data show that locally, significant metal temperature suppression can be obtained by selective application of thermal barrier coatings.

3.6. Sensitivity to uncertainties in external heat transfer coefficient

The prediction of local heat transfer coefficients over a gas turbine blade is very crucial for the prediction of metal temperatures. Accurate data are difficult to obtain because the flow is very complex. An extensive literature survey revealed that there is considerable variation in local heat transfer coefficient from different investigations which in turn suggests that prediction of blade metal temperatures would be subject to uncertainties. Numerical simulations were carried out using external heat transfer coefficients reported by different researchers with convection and combined convection and radiation boundary conditions. Both coated and uncoated blades were studied.

The computations were carried out with six different data sets of the external heat transfer coefficient. All these data are shown in Fig. 2. For the blade shown in Fig. 1, experimental values of heat transfer coefficient are available [19]. Four different data sets have been reported—at two turbulence intensities (4% and 0.4%) and at two Reynolds numbers (4.8×10^5 and 1.3×10^6). The same blade geometry was adopted for numerically predicting the heat transfer coefficient variation along the blade surfaces [24]. Their simulations were performed using 4.2% turbulence intensity and Reynolds numbers of 4.8×10^5, 6.7×10^5 and 1.3×10^6; in the present comparisons, data for the highest Reynolds number was used as it is more representative of actual conditions prevailing in gas turbines. Finally, a typical variation of heat transfer coefficient [20] was also used. Fig. 2 shows that there is considerable variation in the local heat transfer coefficient as obtained from these different sources. For the case of 1.3×10^6 Reynolds number and 4% turbulence intensity, there is a 25% variation between experimental and numerical simulation values along the suction surface. This data also brings out the type of uncertainties existing in local heat transfer coefficient which blade designers have to

Table 1
Select nodal temperatures for different convection heat transfer data

Node	Convection heat transfer data source	[Nodal temperature (K)]			
		[Uncoated blade]		[Coated blade]	
		Convection	Convection and radiation	Convection	Convection and radiation
4	Mukherjee [20]	1313	1344	1369	1380
	Rodi ($\tau = 4\%, Re = 1.3 \times 10^6$) [24]	1288	1325	1341	1356
	Daniels ($\tau = 0.4\%, Re = 4.8 \times 10^5$) [19]	1153	1233	1248	1281
	Daniels ($\tau = 0.4\%, Re = 1.3 \times 10^6$) [19]	1212	1272	1252	1282
	Daniels ($\tau = 4.0\%, Re = 4.8 \times 10^5$) [19]	1212	1272	1294	1317
	Daniels ($\tau = 4.0\%, Re = 1.3 \times 10^6$) [19]	1253	1300	1266	1292
16	Mukherjee [20]	1283	1314	1223	1234
	Rodi ($\tau = 4\%, Re = 1.3 \times 10^6$) [24]	1260	1298	1203	1218
	Daniels ($\tau = 0.4\%, Re = 4.8 \times 10^5$) [19]	1120	1201	1098	1131
	Daniels ($\tau = 0.4\%, Re = 1.3 \times 10^6$) [19]	1191	1248	1155	1177
	Daniels ($\tau = 4.0\%, Re = 4.8 \times 10^5$) [19]	1178	1240	1144	1168
	Daniels ($\tau = 4.0\%, Re = 1.3 \times 10^6$) [19]	1236	1280	1187	1204
82	Mukherjee [20]	1268	1300	1301	1315
	Rodi ($\tau = 4\%, Re = 1.3 \times 10^6$) [24]	1294	1322	1357	1366
	Daniels ($\tau = 0.4\%, Re = 4.8 \times 10^5$) [19]	1060	1152	1082	1133
	Daniels ($\tau = 0.4\%, Re = 1.3 \times 10^6$) [19]	1212	1259	1258	1279
	Daniels ($\tau = 4.0\%, Re = 4.8 \times 10^5$) [19]	1069	1158	1078	1129
	Daniels ($\tau = 4.0\%, Re = 1.3 \times 10^6$) [19]	1281	1312	1333	1345
268	Mukherjee [20]	1237	1262	1167	1175
	Rodi ($\tau = 4\%, Re = 1.3 \times 10^6$) [24]	1212	1242	1151	1161
	Daniels ($\tau = 0.4\%, Re = 4.8 \times 10^5$) [19]	1064	1132	1039	1066
	Daniels ($\tau = 0.4\%, Re = 1.3 \times 10^6$) [19]	1187	1223	1134	1146
	Daniels ($\tau = 4.0\%, Re = 4.8 \times 10^5$) [19]	1058	1127	1035	1062
	Daniels ($\tau = 4.0\%, Re = 1.3 \times 10^6$) [19]	1191	1226	1137	1148
611	Mukherjee [20]	1400	1417	1418	1424
	Rodi ($\tau = 4\%, Re = 1.3 \times 10^6$) [24]	1386	1406	1402	1410
	Daniels ($\tau = 0.4\%, Re = 4.8 \times 10^5$) [19]	1217	1304	1262	1303
	Daniels ($\tau = 0.4\%, Re = 1.3 \times 10^6$) [19]	1374	1398	1391	1401
	Daniels ($\tau = 4.0\%, Re = 4.8 \times 10^5$) [19]	1257	1325	1295	1327
	Daniels ($\tau = 4.0\%, Re = 1.3 \times 10^6$) [19]	1361	1388	1374	1387

consider. Simulations were carried out separately for coated and uncoated blades; in each case two boundary conditions on the external surfaces, viz., convection alone and combined convection–radiation, have been used. Each of these four combinations of coating and boundary condition has been used individually with each of the six sets of heat transfer coefficient data described above. For comparison, data at five select nodes from representative regions in the blade are presented. The exact locations of these nodes are shown in Fig. 1. Nodes 4 and 611 are surface nodes at the leading and trailing edges, respectively. Node 82 is located on the suction surface where the corresponding x/s value is 0.2, a region where changes in heat transfer coefficient are significant. Two more nodes, 16 and 268, located inside the blade, have been selected because they represent typical regions near the leading edge and blade center. Computed temperatures at these five nodes using the six heat transfer coefficient data sets are presented in Table 1.

Table 1 shows that heat transfer coefficient data at Reynolds number 4.8×10^5 consistently yields significantly lower temperatures at all nodes, for the four combinations. This observation is consistent with the data shown in Fig. 2 because at this Reynolds number, the local heat transfer coefficient is lower than the other data over a substantial portion of the pressure and suction surfaces. For this reason, the other four sets of heat transfer data have been used in the following discussion.

For an uncoated blade with convection only, there is a variation of 83–112 K at nodes 4, 16 and 82, all of which are near the leading edge. Node 82 experiences a transitional boundary layer and, consequently, exhibits

large uncertainties in metal temperature. In contrast, node 611 near the trailing edge is affected to the tune of 39 K only. In general, these nodes run hotter than other nodes and, hence, are not strongly affected by variations in the heat transfer coefficient. Uncertainties in temperatures at internal node 268 is about 50 K. However, in the presence of radiation, the radiation component dominates and the uncertainty in the prediction of all the above nodal temperatures decreases, as can be seen from Table 1.

The coated blade with convection only shows variation of 15–143 K at the selected nodes. Out of these, the internal nodes (16 and 268) along with the node in the trailing edge region (611) experience uncertainties ranging from 15 to 69 K which are significantly lower than corresponding values for the uncoated blade. However, the opposite trend is observed for the nodes located on the external surface of the blade. The variations in these cases range from 44 to 143 K. In the presence of radiation, uncertainties at all nodal temperatures decrease by 10–20 K. Nodal temperature uncertainties at the trailing edge in the presence of radiation are even smaller as this region operates at elevated temperatures.

Using the nodal temperature data, the blade effectiveness and heat transfer rate into the blade have been calculated for each case and the results are presented in Tables 2 and 3, respectively. The effectiveness has been defined as the ratio of the difference in gas temperature and the average metal temperature to the difference in gas and cooling air temperature. The effectiveness for Reynolds number 4.8×10^5 is substantially greater than those for the other cases and the heat transfer rate is substantially lower. Table 2 also shows that uncertainties

Table 2
Effectiveness values for different convection heat transfer data

Heat transfer coefficient data source	[Effectiveness]			
	[Uncoated blade]		[Coated blade]	
	Convection	Convection and radiation	Convection	Convection and radiation
Mukherjee [20]	0.36	0.32	0.44	0.43
Rodi and Scheuerer [24] ($\tau = 4\%, Re = 1.3 \times 10^6$)	0.39	0.34	0.47	0.45
Daniels and Browne [19] ($\tau = 0.4\%, Re = 4.8 \times 10^5$)	0.65	0.53	0.68	0.62
Daniels and Browne [19] ($\tau = 0.4\%, Re = 1.3 \times 10^6$)	0.46	0.39	0.51	0.49
Daniels and Browne [19] ($\tau = 4.0\%, Re = 4.8 \times 10^5$)	0.62	0.51	0.65	0.60
Daniels and Browne [19] ($\tau = 4.0\%, Re = 1.3 \times 10^6$)	0.41	0.36	0.48	0.46

Table 3
Heat transfer rates to blade for different convection heat transfer data

Heat transfer coefficient data source	[Heat input per meter blade length (kW/m)]			
	[Uncoated blade]		[Coated blade]	
	Convection	Convection and radiation	Convection	Convection and radiation
Mukherjee [20]	43.6	46.6	36.3	37.3
Rodi and Scheuerer [24] ($\tau = 4\%, Re = 1.3 \times 10^6$)	41.4	44.8	34.7	35.9
Daniels and Browne [19] ($\tau = 0.4\%, Re = 4.8 \times 10^5$)	22.4	31.0	20.2	23.6
Daniels and Browne [19] ($\tau = 0.4\%, Re = 1.3 \times 10^6$)	37.9	42.1	32.2	33.7
Daniels and Browne [19] ($\tau = 4.0\%, Re = 4.8 \times 10^5$)	25.2	32.9	22.6	25.6
Daniels and Browne [19] ($\tau = 4.0\%, Re = 1.3 \times 10^6$)	40.4	44.0	34.2	35.4

in effectiveness are greater for uncoated blade as compared to the coated blade, irrespective of whether radiation is considered. The maximum deviation on the effectiveness due to the different heat transfer coefficient data for coated blade is 0.07 for convection boundary condition and 0.06 for combined convection–radiation boundary condition. The corresponding values for the uncoated case are 0.10 and 0.07, respectively. Similarly, the maximum deviation of the heat transfer rate to the blade for coated blade is 4.1 kW/m for convection boundary condition and 3.6 kW/m for combined convection–radiation boundary condition. The corresponding values for the uncoated case are 5.7 and 4.5 kW/m, respectively, Table 3.

From the foregoing discussion it is clear that the coating acts as a thermal barrier preventing the propagation of heat transfer coefficient uncertainties. In all cases, the presence of radiation dominates heat transfer to the blade and, consequently, the uncertainty in effectiveness is reduced. In other words, metal temperatures in the presence of radiation and/or coating are less sensitive to convection heat transfer coefficient uncertainties. As mentioned earlier, the simulation results with the heat transfer coefficient data at low Reynolds number have not been considered for the above analysis. It has, however, been observed that in the presence of radiation and/or thermal barrier coating, uncertainties in metal temperature predictions are further reduced when convection heat transfer rate is less as compared to radiation heat transfer rate. In the current simulations, these conditions are realized at either Reynolds number 4.8×10^5 or at greater values of TET. At higher values of TET, the effect of radiation and/or coating becomes more pronounced suggesting that larger uncertainties in convection heat transfer coefficient on the external surfaces can be tolerated.

4. Conclusions

The foregoing discussion gives insights into several new aspects of steady state gas turbine blade heat transfer, viz., effects of radiation, TBCs, selective coatings, emissivity uncertainty and uncertainties in convection heat transfer. Radiation heat transfer from gas to blade is significant at TETs of 1500 K and more. TBCs are very effective in blocking radiation, lowering metal temperatures and reducing heat loss to the coolant. All these effects are more pronounced at higher TETs. There is, therefore, considerable scope for reducing coolant flow to the advantage of turbine/cycle efficiency. Localized suppression of metal temperatures is possible by selective local application of TBCs. As compared to coated blades, metal temperatures in the absence of TBCs are, in general, more strongly affected by uncertainties in local heat transfer coefficients on the pressure and suction surfaces. Also, with the inclusion of radiation, it is found that the metal temperatures are less strongly affected by uncertainties.

References

[1] S. Amagasa, K. Shimomura, M. Kadowaki, K. Takeishi, H. Kawai, S. Aoki, K. Aoyama, Study on the turbine vane and blade for a 1500 °C class industrial gas turbine, ASME J. Eng. Gas Turb. Power 116 (1994) 597–604.

[2] N. Kizuka, K. Sagae, S. Anzai, S. Marushima, T. Ikeguchi, K. Kawaike, Conceptual design of the cooling system for 1700°C-class hydrogen-fueled combustion gas turbines, ASME J. Eng. Gas Turb. Power 121 (1999) 108–115.

[3] S. Aoki, K. Teshima, M. Arai, H. Yamao, Results from the phase II test using the high-temperature developing unit (HTDU), ASME J. Eng. Gas Turb. Power 110 (1988) 251–258.

[4] M. Arai, T. Imai, K. Teshima, A. Koga, Research and Development on the HPT of the AGTJ-100B, ASME J. Eng. Gas Turb. Power 110 (1988) 259–264.

[5] G.D. Smith, Thermal barrier characteristics of partially stabilized zirconia coatings on INCOLOY alloy 909 (a controlled expansion alloy), ASME J. Eng. Gas Turb. Power 113 (1991) 135–139.

[6] T.A. Tietz, W.W. Koshel, Computer code for the calculation of the temperature distribution of cooled turbine blades, in: Proceedings of the International Symposium on Air Breathing Engines, Paper no. ISABE 91-7017, 1991, pp. 184–194.

[7] T. Bahree, A.M. Sharan, J.S. Rao, The design of rotor blades taking into account the combined effects of vibratory and thermal loads, ASME J. Eng. Gas Turb. Power 111 (1989) 610–618.

[8] E.A. Thornton, A.R. Wieting, Finite element methodology for transient conduction/forced-convection thermal analysis, in: Proceedings of the Thermophysics Conference, Orlando, FL, AIAA Paper 79-1100, 1979.

[9] E.A. Thornton, A.R. Wieting, Finite element methodology for thermal analysis of convectively cooled structures, Prog. Aeronaut. Astronaut.: Heat Transfer Thermal Contr. Syst. 60 (1978) 171.

[10] R.L. McKnight, Structural analysis applications, ASME J. Eng. Gas Turb. Power 111 (1989) 271–278.

[11] G. Sturmer, A. Schulz, S. Wittig, Lifetime prediction for ceramic gas turbine components, ASME J. Eng. Gas Turb. Power 115 (1993) 70–75.

[12] K. Honjo, R. Hashimoto, H. Ogiyama, Current status of 300 kW industrial ceramic gas turbine R&D in Japan, ASME J. Eng. Gas Turb. Power 115 (1993) 51–57.

[13] T. Cosack, L. Pawlowski, S. Schneiderbanger, S. Sturlese, Thermal barrier coatings on turbine blades by plasma spraying with improved cooling, ASME J. Eng. Gas Turb. Power 116 (1994) 272–276.

[14] N. Asok Kumar, Numerical simulation of heat transfer to gas turbine blades, Ph.D. Thesis, Department of Mechanical Engineering, IIT Delhi, New Delhi, 1995.

[15] G.L. Erickson, Polycrystalline cast superalloys, properties and selection: irons, steels and high-performance alloys, Metals Handbook, vol. I, 10th ed., 1990, pp. 981–994.
[16] Y.S. Touloukian, C.Y. Ho, D.P. Dewitt, Thermal Radiative Properties—Nonmetallic Solids, TPRC Data Series, vol. 8, 1972, pp. 524–525.
[17] Y.S. Touloukian, C.Y. Ho, E.H. Buyco, Specific Heat of Nonmetallic Solids, TPRC Data Series, vol. 5, 1970, pp. 287–295.
[18] Y.S. Touloukian, C.Y. Ho, R.W. Powell, P.G. Klemens, Thermal Conductivity—Nonmetallic Solids, TPRC Data Series, vol. 2, 1970, pp. 240–249.
[19] L.D. Daniels, W.B. Browne, Calculation of heat transfer rates to gas turbine blades, Int. J. Heat Mass Transfer 24 (5) (1981) 871–879.
[20] D.K. Mukherjee, Stress in turbine blades due to temperature load variation, ASME Paper 78-GT-158, 1978.
[21] S.M. Meier, D.K. Gupta, The evolution of thermal barrier coatings in gas turbine engine applications, ASME J. Eng. Gas Turb. Power 116 (1994) 250–256.
[22] J.C. Han, D.W. Ortman, C.P. Lee, A computer model for gas turbine blade cooling analysis, 82-JPGC-GT-6, 1982, pp. 1–7.
[23] K. Nakakado, T. Machida, H. Miyata, T. Hisamatsu, N. Mori, I. Yuri, Strength design and reliability evaluation of a hybrid ceramic stator vane for industrial gas turbines, ASME J. Eng. Gas Turb. Power 117 (1995) 245–250.
[24] W. Rodi, G. Scheuerer, Calculation of heat transfer to convection-cooled gas turbine blades, ASME J. Eng. Gas Turb. Power 107 (1985) 620–627.
[25] M. DeLucia, C. Lanfranchi, An infrared pyrometry system for monitoring gas turbine blades: development of a computer model and experimental results, ASME J. Eng. Gas Turb. Power 116 (1994) 172–177.